A mechanism for reversible solid-state transitions involving nitro torsion

Yue Gui,[1] Xin Yao,[1] Ilia A. Guzei,[2] Michael M. Aristov,[2] Junguang Yu,[1] Lian Yu*[1,2]

[1] School of Pharmacy and [2] Department of Chemistry, University of Wisconsin-Madison, Madison, Wisconsin 53705, USA.

ABSTRACT: Reversible solid-state transformations are important in stimuli-responsive materials. The current understanding is limited on what kind of structure enables reversible transitions. We report that for molecular solids containing nitro groups, reversible phase transitions can occur if the nitro group is a hydrogen bond (HB) acceptor and has torsional freedom. We use the polymorphs of nifedipine (NIF) to illustrate this phenomenon taking advantage of their different molecular packing but identical chemical structure. NIF has six known polymorphs with four being kinetically stable at 100 K. Upon heating, two polymorphs undergo reversible phase transitions with large volume change, while the others do not. In the transforming structures, the nitro group is a HB acceptor and rotates to optimize HBs to offset loss of close packing, while in the inactive structures, the nitro group has similar torsional freedom but is not engaged in HBs. We test the generality of this phenomenon using all available systems in the Cambridge Structural Database, including NIF's derivative nisoldipine, and suggest possible applications in designing materials with controlled mechanical response.

1. INTRODUCTION

Reversible solid-state phase transitions have important applications in stimuli-responsive materials, including ferroelectrics,[1,2] soft robotics,[3] sensors,[4,5,6] energy storage,[7,8] and molecular mechanical devices.[9,10,11,12,13] In this context, molecular crystals play a significant role given the vast diversity of organic molecules and the ability to synthesize them at high purity and tailor their structures at will.[14] Unfortunately, our understanding is limited on what kind of structure gives rise to easily reversible solid-state transitions. Only a small number of systems in the vast structural space are known to have easily reversible polymorphic transitions: globular molecules forming plastic crystals,[15,16] long-chain alkanes with rotator phases,[17] and amino acids with hydrophobic side chains.[18,19,20] A reversible transition has been observed in an organic semiconductor involving torsion of bulky terminal groups linked to a conjugated benzothiophene core.[21,22] Here we report a mechanism for reversible transitions in nitro-containing molecular solids.

The nitro group is present in numerous organic compounds; nitro-rich materials are important as explosives,[14,23] pharmaceuticals,[24] chemical intermediates[25,26] and nonlinear optics.[27,28] An acceptor of hydrogen bonds (HBs)[29,30] the nitro group has a strong influence on structure formation in molecular solids.[31,32,33] In this role, the nitro group proves to be highly flexible: it has significant torsional freedom[34,35,36] and it can form both one-sided and bifurcated HBs.[37] As we show, this flexibility allows a nitro group to adapt to thermodynamic conditions to enable reversible solid-state transitions.

We use the polymorphs of nifedipine (NIF, Chart 1) in this investigation to directly link the phenomenon of interest to the molecular packing responsible, without complications from different chemical entities. This way of using polymorphs for structure-property studies has a long tradition in solid-state chemistry.[38,39,40,41] NIF is an important model for the 1,4-dihydropyridine (DHP) family of calcium channel blockers for treating hypertension[42] and is polymorphic.[43,44,45,46,47] Because of its many torsional degrees of freedom and many HB acceptors but only one donor (the amino H, see Chart 1), NIF exhibits rich conformational polymorphism[48] with diverse HB motifs. NIF has 6 polymorphs with 4 being kinetically stable at 100 K (two discovered in this work, see below). We find that upon heating, two polymorphs (β and γ) undergo reversible phase transitions, but the others (α and δ) do not. In β and γ NIF, the nitro group adjusts its orientation at the phase transition to form stronger HBs and counter the loss of close packing. In α and δ NIF, the nitro group has similar freedom but is not hydrogen-bound and no phase transition occurs. We show literature examples to demonstrate the generality of this phenomenon and discuss its applications in materials design.

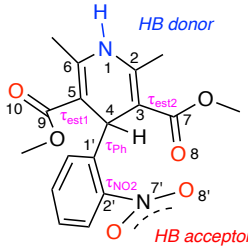

Chart 1. Molecular structure of nifedipine (NIF). The torsion angles indicate sites of conformational freedom: τ_{Ph} (C5-C4-C1'-C2'), τ_{NO2} (C1'-C2'-N7'-O8'), τ_{est1} (C6-C5-C9-O10), and τ_{est2} (C2-C3-C7-O8). An ester group is *cis* if $\tau_{est} \approx 0°$ and *trans* if $\tau_{est} \approx \pm 180°$. The phenyl orientation is *synperiplanar* (*sp*) if the nitro group points in the same direction as C4-H and *antiperiplanar* (*ap*) if it points in the opposite direction. NIF has many HB acceptors (red) but only one donor (blue).

2. RESULTS

2.1. Polymorphs of NIF. Six polymorphs of NIF are known at present, including two discovered in this work. The structures of all these polymorphs have been solved (4 solved in this work) and are described in Table 1, Figure 1, and the deposited Crystallographic Information Files (CIF). By solution and melt crystallization, previous work observed 4 polymorphs: α,[44] β,[47] β' (high-temperature form of β),[47] and γ'.[45] This work discovered a low-temperature form of γ' (named γ). Furthermore, by seeding with a structurally related compound ("pseudo-seeding"),[49,50] another polymorph, δ, was discovered. The idea of pseudo-seeding was inspired by the fact that all NIF polymorphs prior to this work contain the "*cis*/*trans* conformer" (Chart 1), but the "*cis*/*cis* conformer" is present in the crystals of NIF analogs such as felodipine[51] and is statistically favored if an *ortho*-substituent is present on the phenyl ring.[52] This led us to seed felodipine crystals in an NIF melt and to observe the δ polymorph, in which NIF is indeed the *cis/cis* conformer. Given the emphasis of this work, we shall not pursue this aspect of NIF polymorphs here and only use the new structure to establish the origin for reversible transitions.

The NIF polymorphs have rich conformational diversity and hydrogen bonding motifs. At 100 K, four polymorphs are kinetically stable in which the molecule has a variety of conformations (Figure 1A; see Table S1 for the torsion angles). Most polymorphs contain the *cis*/*trans* conformer but the *cis*/*cis* conformer is present in the δ polymorph. These two conformations correspond to the two energy minima with respect to ester torsion (Figure 1B), with the *cis*/*cis* conformer having lower energy by 12 kJ/mol, consistent with the results on similar DHP compounds.[53] That is, before the discovery of δ NIF by pseudo seeding, all known polymorphs contain the high-energy *cis*/*trans* conformer. In addition to ester torsion, the nitro group shows significant freedom. In Figure 1C, we indicate the observed nitro torsion angles on the potential energy surface for nitro torsion. This energy surface has two adjacent minima separated by a low barrier, a consequence of the DHP ring at the *ortho*-position, and all observed nitro torsion angles are clustered around these two minima. As we discuss later, the torsional freedom of the nitro group created by *ortho*-substitution is an important enabler of reversible solid-state transitions.

NIF has many HB acceptors but only one donor – the amino group (Chart 1), and this leads to several bonding motifs in crystals. In the α and δ structures, the amino group binds to an ester group (dashed lines in Figure 1A), but in the γ and γ' structures, it binds to the nitro group. This indicates that the ester group and the nitro group can both serve as HB acceptors in NIF, consistent with their similar HB basicity constants.[30] Indeed, in the β and β' structures, both groups serve as acceptors for the same amino group. Table 2 summarizes the N···O distances in these HBs. In these structures, the ester···amino interactions are easily recognized as HBs based on bonding geometry, but the nitro···amino interactions also qualify as HBs in terms of the donor···acceptor distances from the survey by Etter and coworkers on nitroanilines.[37]

Upon heating, the four polymorphs stable at 100 K exhibit very different behaviors (Figure 2). For α and δ NIF, normal thermal expansion is observed, with volumetric expansion coefficients (156 ppm/K for α and 212 ppm/K for δ) typical for molecular crystals.[54] In contrast, β and γ NIF show a sudden increase of volume, by 3.2% and 4.7%, respectively, indicating first-order phase transitions. We designate the high-temperature phases β' and γ', respectively.

Besides volume expansion, the phase transitions bring about changes in molecular conformation and HBs. After the β → β' transition, the nitro group in one of the symmetry-independent molecules reorients and becomes disordered (Figure 1A). In the same molecule, the *cis* ester group is also disordered. Meanwhile, HBs are *strengthened* in the high-temperature structure. This is seen from an average shortening of the N(H)···O distance by 0.10 Å for the ester···amino interaction and by 0.063 Å for the nitro···amino interaction (Table 2). We observe similar changes occur at the γ → γ' transition: the nitro group reorients after transition (Figure 1A); in one of the two symmetry-independent molecules, the amino H goes from bifurcated bonding to the nitro group to one-sided bonding; the *trans* carbonyl group develops disorder. Meanwhile, the HB network becomes *stronger*, as seen from the average shortening of the N(H)···O(N) distance in the γ' structure by 0.28 Å (Table 2). In both cases (β → β' and γ → γ'), the strengthening of HBs and the creation of disorder likely compensate for the loss of close packing, leading to an overall decrease of free energy.

Table 3 and Figure 3 show the thermodynamic properties of NIF polymorphs. The α polymorph is the most stable solid phase at any temperature. The double-sided arrows indicate reversible polymorphic conversions β ↔ β' and γ ↔ γ' discussed in detail below. Besides these two enantiotropic pairs, another two polymorphs, β' and δ, are enantiotropic, but no reversible transitions have been observed between them. This provides further constraints for possible explanations for reversible phase transitions (see below).

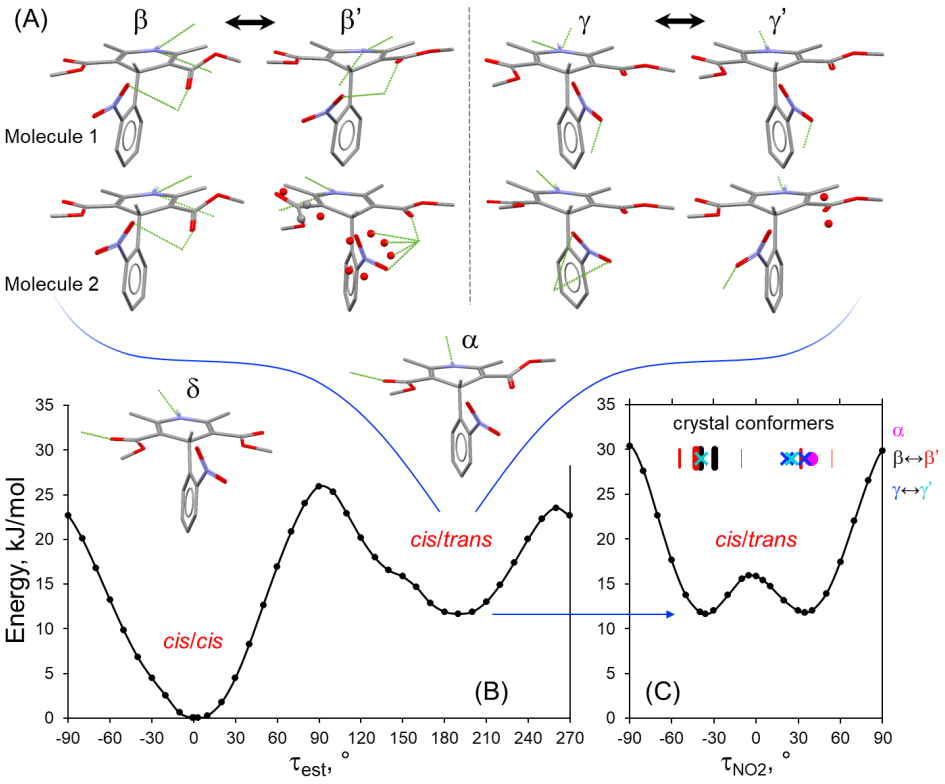

Figure 1. (A) Molecular conformations in NIF polymorphs. There is one symmetry-independent molecule in α and δ, but 2 in the other polymorphs. Double-sided arrows indicate reversible phase transitions. Disorder is present in high-temperature structures β' and γ'. Each green line indicates a HB. Given that the two ester groups are inequivalent in the crystal (unlike the case in solution[55]), each NIF molecule is a chiral object and we compare the molecules in the same "chirality" defined as a *clockwise* rotation while viewing down the C4-H bond (Chart 1) and tracing from the *trans* ester to the *cis* ester and then to the phenyl ring. For a *cis*/*cis* conformer (δ NIF only), the clockwise tracing is from the ester group not engaged in HB to the ester group engaged in HB and then to the phenyl ring. H is omitted except for the amino H and the chirality-defining C4-H. (B) and (C) Torsional energy *E* calculated using B3LYP/6-31G(d). (B) *E* vs. τ_{est}. In this calculation one ester torsion is scanned while the other is left at the *cis* conformation and free to vary. The *cis*/*cis* conformer has lower energy than the *cis*/*trans* by 12 kJ/mol, even though the latter is adopted by most polymorphs. (C) *E* vs τ_{NO2}. In this calculation, the molecule is *cis*/*trans* while scanning τ_{NO2}. Note the two minima separated by a low barrier (4 kJ/mol) each populated by conformers observed in crystals (symbols). For the disordered β' structure the width of the vertical line represents occupancy.

Table 1. Crystal structures of NIF polymorphs.[a]

Form	α		β		β'	γ	γ'		δ	
T, K	100	297	100	296	338	100	250	296	100	293
Ref./CSD	this work	this work	BICCIZ02	BICCIZ03	this work	this work	this work	this work	this work	this work
a, Å	10.567	10.929	9.666	9.840	9.696	19.065	11.435	11.450	11.905	12.025
b, Å	10.408	10.304	13.701	13.807	14.231	11.506	12.244	12.301	10.908	11.238
c, Å	14.788	14.812	14.118	14.206	14.463	15.109	12.327	12.356	12.779	12.827
α, deg	90	90	61.03	61.39	61.90	90	75.54	75.63	90	90
β, deg	95.03	93.17	79.63	79.76	80.40	108.96	89.06	89.09	106.98	107.65
γ, deg	90	90	81.90	81.99	81.80	90	84.77	84.93	90	90
V, Å^3	1620.15	1665.47	1605.89	1664.10	1731.05	3134.48	1664.21	1679.19	1587.14	1651.84
sp grp	$P2_1/c$	$P2_1/c$	$P\bar{1}$	$P\bar{1}$	$P\bar{1}$	$P2_1/c$	$P\bar{1}$	$P\bar{1}$	$P2_1/n$	$P2_1/n$
ρ, g/cm^3	1.420	1.381	1.432	1.382	1.329	1.468	1.382	1.370	1.449	1.393
Z/*Z*'	4/1	4/1	4/2	4/2	4/2	8/2	4/2	4/2	4/1	4/1
R %	3.55	4.73	4.39	5.47	6.69	5.76	4.63	4.38	3.82	4.35

[a] Molecular formula: $C_{17}H_{18}N_2O_6$. Molecular weight: 346.33. See the CSD for the complete list of NIF structures under Ref. Code BICCIZ. Our γ structure is consistent with BICCIZ04[56] but has a smaller R factor.

Table 2. Hydrogen bonding in NIF polymorphs.[a]

	T, K	Ester···amino HB $R_{N\cdots O(C)}$, Å	Nitro···amino HB $R_{N\cdots O(N)}$, Å
α	100	2.958(1)	none
	297	3.032(3)	
δ	100	2.992(1)	
	293	3.079(2)	
β	100	2.993(2) mol. 1; 3.033(2) mol. 2	3.181(2) mol. 1; 3.439(2) mol. 2
	296	3.040(3) mol. 1; 3.093(3) mol. 2	3.279(4) mol. 1; 3.525(4) mol. 2
β'	338	2.903(6) mol. 1; 3.022(6) mol. 2 ΔR = -0.10	3.402(7) mol. 1; 3.296(11) [46%], 3.209(12) [34%], 2.913(8) [11%], 3.87(6) [9%] mol. 2 ΔR = -0.063
γ	100	none	3.203(3) mol. 1; 3.528(3)/3.646(3) bifurcated, mol. 2
γ'	250	none	3.231(2) mol. 1; 3.005(2) mol. 2 ΔR = -0.28
	296	none	3.247(2) mol. 1 3.018(2) mol. 2

[a] "mol. 1" and "mol. 2" signify molecules 1 and 2 in a Z' = 2 structure. ΔR is the average change of the N···O distance. For β' NIF, the multiple distances for the nitro···amino HB reflect disordered nitro orientations for which % occupancies are given.

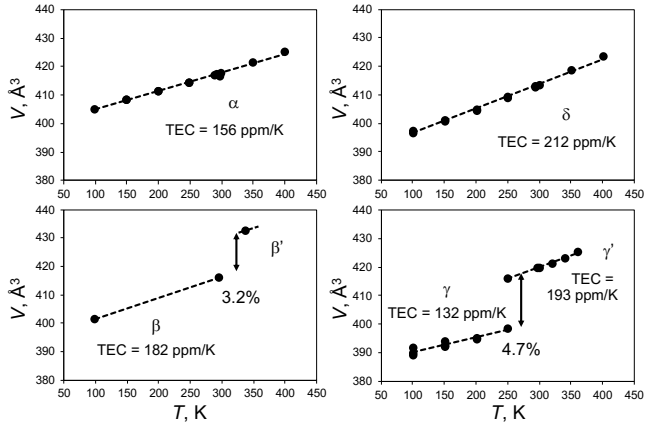

Figure 2. Molecular volume as a function of temperature in NIF polymorphs. Normal thermal expansion coefficient (TEC) is observed in α and δ NIF, while the β and γ curves show discontinuity, indicating first-order phase transitions with volume expansion. The short dashed line for β' NIF indicates estimated TEC, which could not be measured due to fast conversion to the α phase.

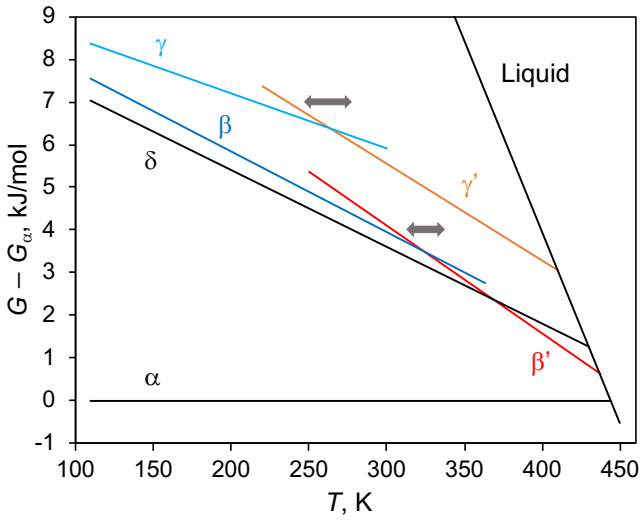

Figure 3. Free energies of NIF polymorphs relative to α NIF. The calculation was made using the temperatures and enthalpies of phase transitions (Table 3) and standard thermodynamic equations.[57] The α polymorph is the most stable at any temperature. The double-sided arrows indicate reversible polymorphic conversions.

Table 3. Thermodynamic properties of NIF polymorphs.

Form	α	β'	γ'	δ
T_m, K	444	437	410	430
ΔH_m, kJ/mol	39.8 [a]	28.1	27.4	30.8

Solid-state transformation	β → β'	γ → γ'
T_t, K	326 [b]	264 [c]
ΔH_t, kJ/mol	2.1	2.6
$\Delta\rho$	3.2%	4.7%

[a] Consistent with literature values (36.0 to 39.9 kJ/mol).[58,59] [b] Average transition onset temperatures during cooling (318 K) and heating (333 K) at 2 K/min; see Figure 4A. [c] Average transition onset temperatures during the first cooling (247 K) and the first heating (281 K) at 2 K/min; see Figure 5A.

2.2. Reversible phase transitions β ↔ β' and γ ↔ γ'. A remarkable property of NIF polymorphs is that four structures are stable at 100 K (α, β, γ, and δ), and two of them (β and γ) undergo reversible solid-state transitions upon heating, while the other two (α and δ) do not. This situation is highly unusual since in most systems showing reversible solid-state transitions, the transitions are serial in temperature, with no parallel pathways as seen in NIF. These parallel pathways provide a strong test of the transition mechanism.

Figure 4A shows the Differential Scanning Calorimetry (DSC) traces of the β ↔ β' transition measured with a lightly ground powder. The transition during heating occurs at 333 K with absorption of heat, while the transition during cooling occurs at 318 K with release of heat. These transitions are first-order with significant latent heat (2.1 kJ/mol) and volume change (3.2%). In spite of this, the transition is easily reversible many times

without fatigue. An intriguing feature is that while the temperature hysteresis is sizable (15 K), increasing the scan rate from 2 to 10 K/min has no effect on the transition temperatures.

Figure 4B shows the photomicrographs of the β ↔ β' transition extracted from a video (see Video S1). A single crystal of β NIF was heated from 298 K to 335 K at 10 K/min and cooled to 298 K at 10 K/min. A phase transition occurs abruptly at 333 K in less than 70 ms (two video frames) with sudden change of birefringence and lengthening of the crystal (from 205 to 210 μm). Upon cooling, the reverse transition occurs at 316 K in 140 ms (4 video frames). The heating and cooling transitions are both single-crystal-to-single-crystal with no obvious damage of the crystal, consistent with the reversibility of thermal events in Figure 4A. It was noticed that crystal size influenced whether the phase transition is single-crystal-to-single-crystal and that crystals larger than 500 μm could crack during transition.

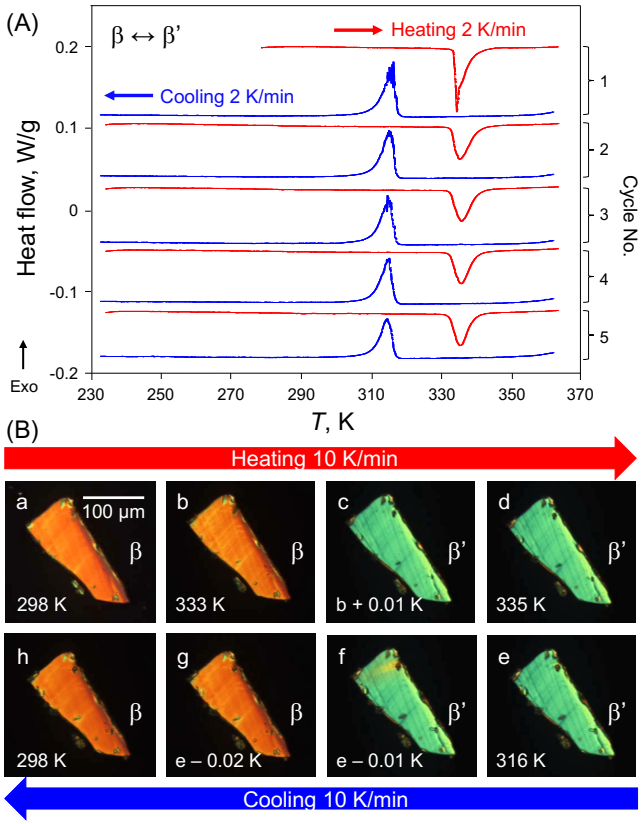

Figure 4. Reversible β ↔ β' transition in NIF. (A) DSC heat/cool cycles indicate easy reversibility without fatigue. (B) Photomicrographs of the transition extracted from a video (Video S1). Top row: heating from 298 K to 335 K at 10 K/min. A β single crystal transforms to β' at 333 K (b to c) with a change of birefringence and an increase of its length. Bottom row: cooling from 335 K to 298 K at 10 K/min. The reverse process occurs at 316 K (f to g).

Similar to the β polymorph, the γ polymorph undergoes reversible transition upon heating. Figure 5A shows the DSC traces for the γ ↔ γ' transition. The transition is endothermic on heating and exothermic on cooling. It is repeatable many times, but the reversibility is somewhat worse relative to the β ↔ β' transition. With each heat/cool cycle, the up-transition temperature rises and the down-transition temperature falls, increasing the hysteresis; meanwhile, the enthalpy of transition decreases gradually, from 2.6 kJ/mol in the first heating to 1.7 kJ/mol in the fifth. Another feature of the γ ↔ γ' transition is that the DSC trace has sharp peaks in early cycles, but is smooth in later cycles. This is caused by crystal fracture, as discussed below.

Figure 5B shows the photomicrographs of the γ ↔ γ' transitions extracted from a video (Video S2). A single crystal of the high-temperature form γ' was cooled from 298 K to 200 K at 10 K/min and heated to 298 K at 10 K/min. A phase transition occurs during cooling at 244 K with sudden change of birefringence and fracture of the crystal. The 244 K transition temperature observed in this single crystal agrees with that detected by DSC in the first cooling (247 K). Upon reheating, the reverse transition occurs at 285 K, also consistent with the DSC result (281 K). The crystal fracture during transition is responsible for the sharp peaks in the DSC trace (Figure 5A). As large crystals break into small ones, individual fracture events are no longer resolved, leading to smooth heat flow. Similar result has been observed with L-pyroglutamic acid where large crystals show spiky DSC traces during phase transition, while the spikes vanish after grinding.[60]

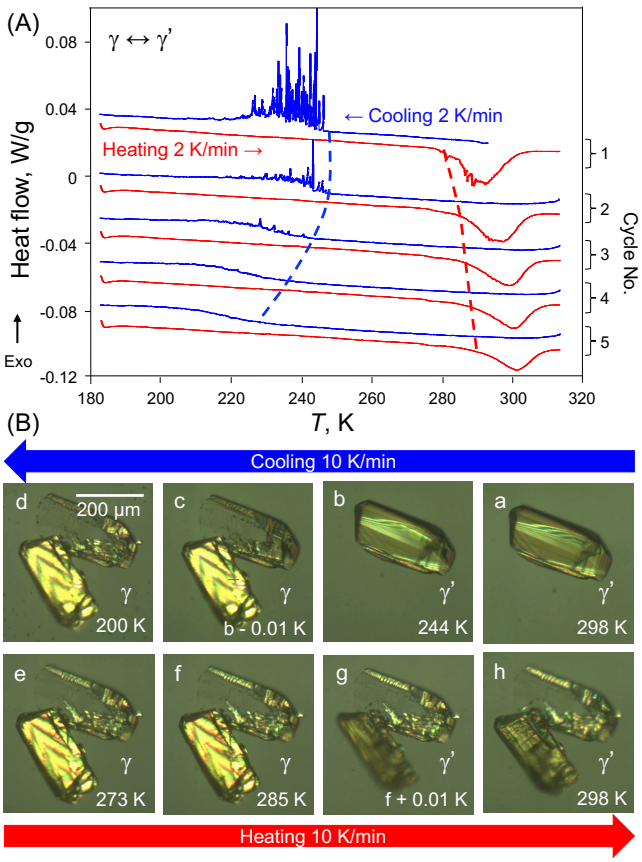

Figure 5. Reversible γ ↔ γ' transition in NIF. (A) DSC heat/cool cycles indicate reversibility, as well as increasing hysteresis (see the dashed curves tracing the onset temperatures) and diminishing intensity. (B) Photomicrographs of the transition extracted from a video (Video S2). Top row: cooling from 298 K to 200 K at 10 K/min. A single crystal of γ' transforms to γ at 244 K (b to c) with change of birefringence and fracture of the crystal. Bottom row: heating from 200 K to 298 K at 10 K/min. The reverse transition occurs at 285 K (f to g).

2.3. Reversible phase transitions in nisoldipine. Similar reversible phase transitions were observed in a derivative of NIF, nisoldipine (NIS, Figure 6A). NIS and NIF have very similar structures, with the only difference being the replacement of a methyl ester in NIF by an isobutyl ester in NIS. Only one crystal structure is known for NIS at the time of this work (CSD ref. code FULPAD; Table S2).[61] This structure is similar to that of β NIF, in which the amino H is hydrogen bound to both the nitro and an ester group (Figure 6B). We therefore expect NIS to undergo similar reversible phase transitions as β NIF. This is indeed the case. As Figure 6C shows, NIS undergoes an endothermic transition upon heating with a latent heat of 7 J/g and an exothermic transition upon subsequent cooling. The transition can be repeated without fatigue, as in the case of β NIF. A difference between the two systems is that the transition in NIS is more gradual and occurs at a higher temperature, near the crystal melting point (422 K).

As in the case of NIF, the reversible transition in NIS is associated with disordering in the high temperature structure. While the 293 K structure shows no positional disorder, the 400 K structure is disordered at the nitrophenyl and isobutyl sites (see Figure 6B and the deposited CIF files). Figure 6D shows the molecular volume of NIS as a function of temperature. Below 300 K, normal thermal expansion is observed (TEC = 149 ppm/K); above 300 K, expansion is significantly faster with an apparent TEC being 2.3 times larger than the low temperature value. It is noteworthy that the data in the transition zone were collected during both heating and cooling. Their agreement indicates a reversible phase transition, consistent with the DSC result.

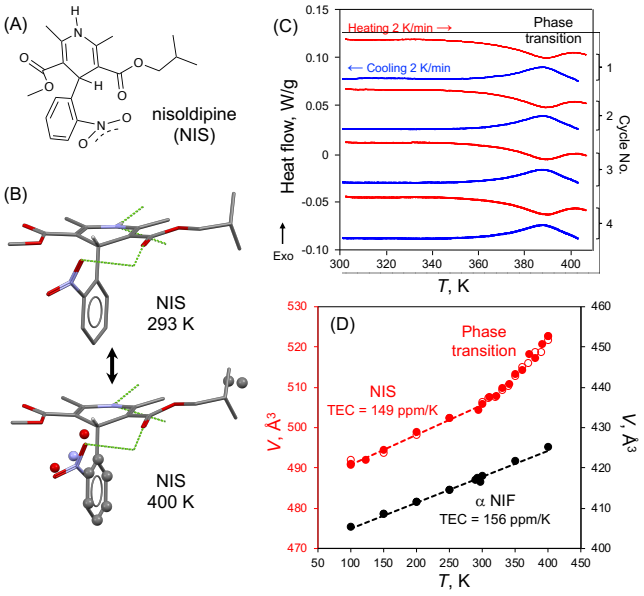

Figure 6. (A) Molecular structure of NIS. (B) Effect of phase transition on the conformation of NIS. Disorder is present in the high-temperature structure. Each green line indicates a HB. (C) DSC heat/cool cycles indicate reversible transitions without fatigue. (D) Molecular volume of NIS as a function of temperature. Normal thermal expansion is observed below 300 K (TEC = 149 ppm/K, comparable with the value for α NIF, 156 ppm/K), but "abnormal" expansion is seen during phase transition with the apparent TEC being 2.3 times larger. In the transition zone, data were collected during both heating (solid symbols) and cooling (open symbols), indicating reversibility of the transition.

3. DISCUSSION

We have observed that two NIF polymorphs (β and γ) show reversible solid-state phase transitions, but the others (α and δ) do not. The essential difference between the two sets of polymorphs is that in β and γ NIF, the nitro group is a HB acceptor and it reorients during transition, leading to stronger HBs. In the α and δ structures, the nitro group is not engaged in HBs and no reversible transitions are observed. In the case of nisoldipine, the low-temperature structure is similar to that of β NIF and it also undergoes reversible transitions upon heating. These easily reversing transitions are in contrast with the suspended transition between enantiotropic polymorphs β' and δ (Figure 3). As we discuss below, these results identify a general mechanism for reversible solid-state transitions that involves nitro torsion and simultaneous optimization of HBs.

Given the importance of nitro torsion in our phenomenon, we first discuss the torsional freedom of the nitro group in NIF. As shown in Figure 1C, the energy profile for nitro torsion consists of two minima at $\tau_{NO2} = \pm 35°$ separated by a low barrier of 4 kJ/mol at $\tau_{NO2} = 0°$. This double-welled energy profile differs from that of the bare nitrobenzene (Figure 7), which has a single well at $\tau_{NO2} = 0°$ surrounded by energy barriers at $\tau_{NO2} = \pm 90°$. This difference arises from steric effect:[35] in nitrobenzene, the nitro group tends to be coplanar with the phenyl ring to maximize π conjugation,[36] but in NIF, the DHP group in the *ortho*-position (Chart 1) blocks the access of the nitro group to coplanarity. The double-welled energy surface creates greater conformational freedom for the nitro group. This is illustrated by the double-sided arrow in Figure 7. At 5 kJ/mol (roughly the thermal energy), the accessible range for τ_{NO2} in NIF is twice that in nitrobenzene. The large conformational freedom of the nitro group in NIF is supported by the wide range of torsion angles in NIF crystals (symbols over the energy curve in Figure 1C), which are all clustered around the two minima.

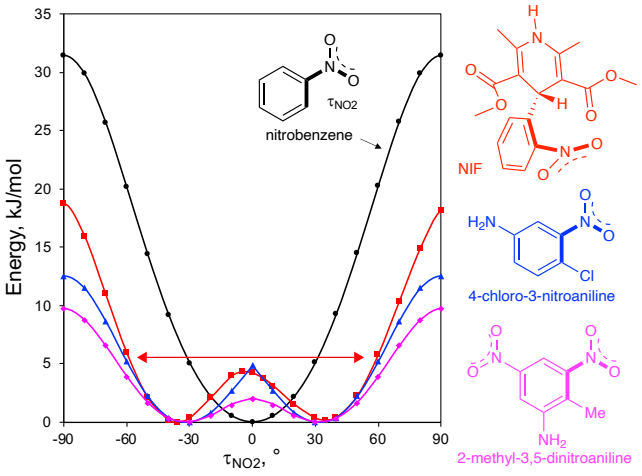

Figure 7. Energy vs nitro torsion angle in NIF and related molecules calculated using B3LYP/6-31G(d). Double-sided arrow indicates increased torsional freedom due to *ortho*-substitution of nitrobenzene. The torsion angle of interest is bolded.

We explain the reversible solid-state transitions in NIF and the related NIS on the basis of the enhanced flexibility of the nitro

group. In the β and γ structures, the nitro group is an acceptor of HBs – the strongest organizing force in these crystals; with changing temperature, strain develops in the HB network and the nitro group makes facile adjustments to ensure optimal geometry between bonding groups. In the α and δ polymorphs, the nitro group is not involved in HBs and its internal rotation, though feasible, has no strong impact on stability. These polymorphs do not show reversible solid-state phase transitions. In the case of δ NIF, transformation is thermodynamically allowed to the β' phase (Figure 3) but none is observed due to the large changes in molecular conformation and HB. This explanation applies equally well to the analog of NIF, NIS (Figure 6). The minor alteration of a distant ester group is not expected to change the energy profile for nitro torsion (Figure 7). The crystal structure of NIS is similar to that of β NIF in which the nitro group is a HB acceptor. Our model predicts similar reversible transitions in both systems, in perfect accord with experiment.

The discussion above suggests a general principle for reversible solid-state transitions: For nitro-containing molecular solids, reversible transitions are expected if (1) the nitro group is a HB acceptor and (2) the nitro group is conformationally flexible. Based on the result on NIF polymorphs, we expect the reversible transition to involve torsion of the nitro group and creation of disorder in the high-temperature phase.

Our results on NIF indicate that both conditions must be satisfied, as all NIF polymorphs should satisfy Condition (2), but only those that satisfy Condition (1) show reversible phase transitions. Conversely, the positional isomers of nitroaniline all satisfy Condition (1) (see Figure S4), but not Condition (2). This is because an *ortho*-substituent is absent in the *para*- and *meta*-isomers, making the nitro-torsion barrier similar to that of the bare nitrobenzene (Figure 7), while the formation of intramolecular HB in *ortho*-nitroaniline elevates the barrier for nitro torsion. According to our model, these systems should not show reversible phase transition and this is indeed the case according to calorimetric[62] and X-ray diffraction measurements[63] from 100 K to melting points.

We now discuss examples where Conditions (1) and (2) are both met and the system shows reversible solid-state transitions. Our goal is to use the entire literature to test our hypothesis. For this purpose, the CSD was searched by combining the keywords "nitro" and "polymorph" or "phase". This returned 849 hits and manual inspection identified 8 (Table 4) that satisfy our two conditions and are predicted to have reversible phase transitions. All these structures contain an *ortho*-substituted nitrobenzene group, as in NIF and NIS, with enhanced conformational freedom (Figure 7). Furthermore, in all these structures, the nitro group is a HB acceptor. One of these 8 hits is γ NIF from this work, now deposited to the CSD. For two of the 8 cases, we found no literature information on phase transitions to test our model. For the remaining 6 cases, *reversible phase transitions have been observed in every case*, as predicted. The reversible transitions in 3 of these structures, β NIF, γ NIF and NIS, have already been described above; we will discuss the remaining 3 cases below.

Table 4. Structures from CSD search that are predicted to have reversible transitions by the nitro-torsion mechanism.

Name	Ref. Code	Consistent with prediction
β NIF	BICCIZ03	Yes
γ NIF	1985173 [a]	Yes
NIS	FULPAD	Yes
4-chloro-3-nitroaniline	ZOXHAX	Yes
4-iodo-3-nitroaniline	ETOJUS	Yes
2-methyl-3,5-dinitroaniline	ISAXUV	Yes
4-methyl-3-nitroaniline	ZZZJIQ	N.A. [b]
4-[(2-nitrophenyl)azo]phenol	YEJNAC	N.A. [b]

[a] Deposition number. [b] No literature information to test the prediction.

We first show that the 3 systems in question satisfy Condition (2). Figure 7 shows the energy profile for nitro torsion in 4-chloro-3-nitroaniline and 2-methy-3,5-dinitroaniline. As in the case of NIF, two energy wells are seen separated by a low barrier. In these molecules, the *ortho*-substituent prevents the nitro group from attaining coplanarity with the phenyl ring, creating the double minima. We expect the profile for 4-iodo-3-nitroanilie to be similar to that for its chloro analog (the nitro-torsion barrier is apparently insensitive to the size of the *ortho*-substituent for the large DHP group in NIF does not lead to high barrier).

In 4-chloro-3-nitroaniline and 4-iodo-3-nitroaniline, the nitro group forms HB with the amino group (Figure 8A). Thus, they also satisfy Condition (1) and according to our model, both should exhibit reversible phase transitions. This is indeed observed: upon heating, each system shows a reversible phase transition with the nitro group developing disorder in the high-temperature phase (Figure 8A).[64]

In the case of 2-methyl-3,5-dinitroaniline, the nitro groups form HBs with the amino group (Figure 8A) and the 3-nitro group (adjacent to methyl) has large conformational freedom (Figure 7), thus meeting both of our conditions. Our model predicts that this system should undergo reversible phase transitions. Indeed, upon heating, the crystal transforms reversibly to a high-temperature structure in which the 3-nitro group is disordered (Figure 8A).[65] An interesting feature of this system is that there are two nitro groups with different degrees of freedom. Because of the adjacent methyl group, the 3-nitro group has a double-welled torsion energy profile similar to that of NIF (Figure 7), but the 5-nitro group (no *ortho*-substituent) has a torsion energy profile similar to that of nitrobenzene. In the high-temperature structure, the 3-nitro group is disordered, while the 5-nitro is not. These results are in complete agreement with our prediction. In summary, our literature search has returned only examples in support of our model and no counterexamples.

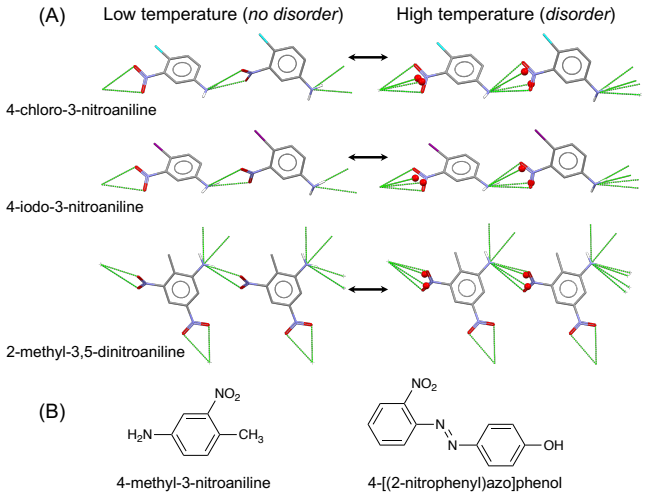

Figure 8. Structures retrieved from the CSD that meet our two conditions and are predicted to have reversible transition by the nitro-torsion mechanism. (A) Reversible solid-state phase transitions in 4-chloro-3-nitroaniline, 4-iodo-3-nitroaniline and 2-methyl-3,5-dinitroaniline. In each case, the nitro group with an *ortho*-substituent participates in hydrogen bonding. Consistent with our model, all three systems exhibit reversible phase transitions during which the nitro group undergoes internal rotation and develops disorder in the high-temperature form. Dashed lines indicate HBs. Display colors: grey for C; red for O; blue for N; cyan for Cl, purple for I, white for H. H is omitted except for the amino H. (B) Two structures that meet our conditions, but have no literature information to test our model.

A further consistency test of the above model is to determine whether the ester groups in NIF are similarly flexible, for if so, our model would predict reversible transitions in the α and δ polymorphs as well, involving the torsion of the hydrogen-bound ester groups. In Figure 1, we compare the energy profiles for nitro torsion and ester torsion. We find that ester torsion is less free than nitro torsion across the double minima. While this comparison is made in the gas phase, the thermal displacement factors of NIF crystal structures confirm larger torsional oscillations of the nitro group relative to the ester group, indicating greater freedom.[34] Thus, the absence of phase transitions in α and δ NIF is fully consistent with the nitro-torsion mechanism of solid-state transformations.

4. CONCLUSIONS

Using the polymorphs of nifedipine, we have demonstrated that a nitro-containing solid material is expected to undergo reversible phase transitions if (1) the nitro group serves as a HB acceptor and (2) the nitro group is conformationally flexible. The use of polymorphs in this context adds considerable weight to the conclusion since the polymorphs differ only in molecular packing and share the same chemical composition. During the phase transition, the nitro group rotates and possibly develops disorder in the high-temperature phase, leading to stronger HBs and higher entropy. This offsets the loss of close packing. The generality of the phenomenon is supported by all available systems in the literature for which our model can be tested, including an analog of nifedipine, nisoldipine. A common feature for all the systems studied is a nitrobenzene core with a non-hydrogen-bonding *ortho*-substituent, which reduces the barrier for nitro torsion and expands its conformational freedom (Figure 7). We expect other molecules of this class to show the same phenomenon, as well as non-nitrobenzene molecules that satisfy the two conditions above. These predictions should be further tested in future work.

The nitro-torsion mechanism for reversible solid-state transitions differs from the other mechanisms previously studied. The transition to a plastic phase of globular molecules[16] requires whole-molecule rotation so that entropy rises to nearly the liquid level. The transition to rotator phases in long-chain alkanes and derivatives[17] similarly involves motions of a large portion of the molecule. The reversible transition in hydrophobic amino acids[19] is characterized by rearrangement in the hydrophobic (van der Waals) region of the structure while the HB motifs remain intact. In contrast, the transitions in the nitro compounds involve the torsion and disordering of a relatively small functional group, while optimizing HBs. This mechanism can be applied to the design of nitro-containing solid materials that undergo reversible solid-state transitions or are free from them. Given that about half of the known polymorphic pairs are enantiotropic[57] and can in principle show reversible transitions, we expect systematic investigations to reveal other mechanisms of reversible solid-state transitions.

The mechanism of fast, reversible solid-state transitions remains poorly understood. Some associate the high speed with a cooperative process,[20,22] while others allow possibilities for a nucleation-and-growth mechanism in which growth rate is very fast.[66,67] Based on simulations, Beckham et al. argue that the fast transition in terephthalic acid leading to "jumping crystals" is initiated by surface nucleation followed by fast growth at ~8 m/s.[67] For NIF, the information is incomplete at present to determine the mechanism of transformation, but there were occasional indications of nucleation sites from which growth fronts propagated. This would suggest a nucleation-and-growth process. Future work is warranted where high-speed photography and simulations are used to examine the transformation process.

5. MATERIALS AND METHODS

Nifedipine [1,4-Dihydro-2,6-dimethyl-4-(2-nitrophenyl)-3,5-pyridinedicarboxylic acid dimethyl ester, NIF, ≥98% pure, polymorph α] was purchased from Sigma Aldrich (St. Louis, MO). Nisoldipine [1,4-Dihydro-2,6-dimethyl-4-(2-nitrophenyl)-3,5-pyridinedicarboxylic acid isobutyl methyl ester, NIS, ≥98% pure] and felodipine [1,4-Dihydro-2,6-dimethyl-4-(2,3-dichlorophenyl)-3,5-pyridinedicarboxylic acid ethyl methyl ester, ≥98% pure, polymorph I] were purchased from Tokyo Chemical Industry Co., Ltd. (TCI).

Single crystals of α NIF for structural solution were grown by slow evaporation from an ethanol solution at the ambient temperature. NIF is light sensitive and all handling and preparation were performed under low light conditions and the samples were protected from light during storage.

β NIF was obtained in two ways: by cross nucleation and by crystallization in the glassy state. In the cross-nucleation method, a melt of NIF was seeded with α NIF crystals at 390 K (controlled with a Linkam THMS 600 hot stage). The resulting crystals at 390 K were the high-temperature polymorph β',

which converted to β on cooling. After preparation, any α seed crystals were removed with a razor blade. The resulting material was a polycrystalline powder. In the second method, single crystals of β NIF for structural solution were grown from a glass of NIF containing 10 wt% TWEEN 20 (polyethylene glycol sorbitan monolaurate, from Sigma Aldrich). The mixture was melted and cooled to produce a solid glass and single crystals of β NIF grew from this glass in 2 days at 298 K. Single crystals of β' NIF were obtained by heating β NIF single crystals above 333 K.

Crystallization of isolated liquid droplets was used to prepare γ' NIF. This method was used because γ' NIF grew slowly and had phase transition when contacting with other polymorphs. Small droplets of liquid NIF were formed on a coverslip by melting the as-purchased material and allowed to crystallize at 373 K. At this temperature, γ' NIF nucleated spontaneously. If it contained several crystals, the droplet was heated near the melting point of γ' NIF (410 K) to melt all but one. The droplet was then heated to 405 K to grow a single crystal. γ NIF was obtained by cooling γ' NIF to below 247 K.

Polycrystalline δ NIF was first obtained by seeding an NIF melt with felodipine Form I crystals at 298 K and crystallizing at 390 K. Then the polycrystals were used as seeds to grow single crystals of δ NIF at 425 K using isolated droplets as described above.

Single crystals of NIS were grown from the melt using the method of isolated micro-droplets. Single-crystal structure was measured by X-ray diffraction as a function of temperature to investigate phase transitions.

DSC was performed with a TA Instruments Q2000 under N_2 purge (50 mL/min). DSC was used to measure the temperatures and enthalpies of phase transitions (T_m, ΔH_m, T_t and ΔH_t in Table 3). Powder X-ray diffraction was performed with a Bruker D8 Advance diffractometer. Raman spectra were obtained with a Thermo Scientific DXR with a 780 nm laser. Light microscopy was performed with an Olympus BH2-UMA equipped with a digital camera. A Bruker Quazar SMART APEX2 diffractometer was used to collect data for solving crystal structures. Measurements were performed in dark to prevent degradation of NIF and NIS. The X-ray source was either Mo K_α (λ = 0.71073 Å) or Cu K_α (λ = 1.54178 Å). See the deposited CIF files under deposition number 1984619, 1984646, 1985173, 1985174, 1985175, 1985177, 1985178, 1985183, 2018451, 2018452 and 2018454 for the details of structural solution, which can be obtained free of charge from the Cambridge Crystallographic Data Centre www.ccdc.cam.ac.uk/structures.

DFT calculations were performed with Gaussian 16 using B3LYP with a 6-31G(d) basis set on WebMO.[68]

ASSOCIATED CONTENT

Supporting Information

Torsion angles of molecules in NIF polymorphs, DFT calculations, videos of reversible β ↔ β'and γ ↔ γ' transitions, Raman spectra of NIF polymorphs including the new δ form, powder X-ray diffraction patterns of NIF polymorphs, crystal structure of NIS, and crystal structures of *para*-, *meta*-, *ortho*-nitroanilines (PDF)
Video of reversible β ↔ β' NIF transition (mov)
Video of reversible γ ↔ γ' NIF transition (mov)
Crystallographic data for α NIF at 100 K (CIF)
Crystallographic data for α NIF at 297 K (CIF)
Crystallographic data for β' NIF at 338 K (CIF)
Crystallographic data for γ NIF at 100 K (CIF)
Crystallographic data for γ' NIF at 250 K (CIF)
Crystallographic data for γ' NIF at 296 K (CIF)
Crystallographic data for δ NIF at 100 K (CIF)
Crystallographic data for δ NIF at 293 K (CIF)
Crystallographic data for NIS at 100 K (CIF)
Crystallographic data for NIS at 293 K (CIF)
Crystallographic data for NIS at 400 K (CIF)

AUTHOR INFORMATION

Corresponding Author

* Lian Yu – School of Pharmacy, University of Wisconsin-Madison, Madison, WI 53705, United States; orcid.org/0000-0002-4253-5658; Email: lian.yu@wisc.edu

Other Authors

Yue Gui – School of Pharmacy, University of Wisconsin-Madison, Madison, WI 53705, United States; orcid.org/0000-0002-4416-3907; Email: ygui@wisc.edu
Xin Yao – School of Pharmacy, University of Wisconsin-Madison, Madison, WI 53705, United States; orcid.org/0000-0002-7657-4997; Email: xyao39@wisc.edu
Ilia A. Guzei – Department of Chemistry, University of Wisconsin-Madison, Madison, Wisconsin 53706, United States; orcid.org/0000-0003-1976-7386; Email: iguzei@chem.wisc.edu
Michael M. Aristov – Department of Chemistry, University of Wisconsin-Madison, Madison, Wisconsin 53706, United States; orcid.org/0000-0003-1161-5126; Email: aristov@wisc.edu
Junguang Yu – School of Pharmacy, University of Wisconsin-Madison, Madison, WI 53705, United States; Email: jyu288@wisc.edu

Notes

The authors declare no competing financial interest.

ACKNOWLEDGMENT

This research was partially supported by NSF through the University of Wisconsin Materials Research Science and Engineering Center (Grant DMR-1720415). Bruker D8 VENTURE Photon III X-ray diffractometer was partially funded by NSF Award CHE-1919350 to the UW–Madison Department of Chemistry. Bruker Quazar APEX2 was purchased by UW–Madison Department of Chemistry with a portion of a generous gift from Paul J. and Margaret M. Bender.

ABBREVIATIONS

NIF, nifedipine; HB, hydrogen bond; DHP, dihydropyridine; DFT, density functional theory; CIF, crystallographic information files; DSC, differential scanning calorimetry; TEC, thermal expansion coefficient; CSD, Cambridge Structural Database.

REFERENCES

[1] Sun. Z.; Chen, T.; Ji. C.; Zhang, S.; Zhao, S.; Hong, M.; Luo, J. High-Performance Switching of Bulk Quadratic Nonlinear Optical Properties with Large Contrast in Polymer Films Based on Organic Hydrogen-Bonded Ferroelectrics. *Chem. Mater.* **2015**, *27*, 4493-4498.

[2] You, Y.-M.; Liao, W.-Q.; Zhao, D.; Ye, H.-Y.; Zhang, Y.; Zhou, Q.; Niu, X.; Wang, J.; Li, P.-F.; Fu, D.-W.; Wang, Z.; Gao, S.; Yang, K.; Liu, J.-M.; Li, J.; Yan, Y.; Xiong, R.-G. An Organic-Inorganic Perovskite Ferroelectric with Large Piezoelectric Response. *Science* **2017**, *357*, 306-309.

[3] Manti, M.; Cacucciolo, V.; Cianchetti, M. Stiffening in Soft Robotics: A Review of the State of the Art. *IEEE Robot. Autom. Lett*. **2016**, *23*, 93-106.

[4] Wenger, O. S. Vapochromism in Organometallic and Coordination Complexes: Chemical Sensors for Volatile Organic Compounds. *Chem. Rev.* **2013**, *113*, 3686-3733.

[5] Mendes, P. M. Stimuli-Responsive Surfaces for Bio-Applications. *Chem. Soc. Rev*. **2008**, *37*, 2512-2529.

[6] Huang, R.-W.; Wei, Y.-S.; Dong, X.-Y.; Wu, X.-H.; Du, C.-X.; Zang, S.-Q.; Mak, T. C. W. Hypersensitive Dual-Function Luminescence Switching of a Silver-Chalcogenolate Cluster-Based Metal-Organic Framework. *Nat. Chem.* **2017**, *9*, 689-697.

[7] Benson, D. K.; Burrows, R. W.; Webb, J. D. Solid State Phase Transitions in Pentaerythritol and Related Polyhydric Alcohols. *Sol. Energy Mater.* **1986**, *13*, 133−152.

[8] Kiyabu, S.; Lowe, J. S.; Ahmed, A.; Siegel, D. J. Computational Screening of Hydration Reactions for Thermal Energy Storage: New Materials and Design Rules. *Chem. Mater.* **2018**, *30*, 2006-2017.

[9] Naumov, P.; Chizhik, S.; Panda, M. K.; Nath, N. K.; Boldyreva, E. Mechanically Responsive Molecular Crystals. *Chem. Rev*. **2015**, *115*, 12440−12490.

[10] Taniguchi, T.; Sugiyama, H.; Uekusa, H.; Shiro, M.; Asahi, T.; Koshima, H. Walking and Rolling of Crystals Induced Thermally by Phase Transition. *Nat. Comm*. **2018**, *9*, 538.

[11] Su, S.-Q.; Kamachi, T.; Yao, Z.-S.; Huang, Y.-G.; Shiota, Y.; Yoshizawa, K.; Azuma, N.; Miyazaki, Y.; Nakano, M.; Maruta, G.; Takeda, S.; Kang, S.; Kanegawa, S.; Sato, O. Assembling an Alkyl Rotor to Access Abrupt and Reversible Crystalline Deformation of a Cobalt(II) Complex. *Nat. Comm.* **2015**, *6*, 8810.

[12] Dharmarwardana, M.; Welch, R. P.; Kwon, S.; Nguyen, V. K.; McCandless, G. T.; Omary, M. A.; Gassensmith, J. J. Thermo-mechanically Responsive Crystalline Organic Cantilever. *Chem. Commun.* **2017**, *53*, 9890–9893.

[13] Sahoo, S. C.; Panda, M. K.; Nath, N. K.; Naumov, P. Biomimetic Crystalline Actuators: Structure-Kinematic Aspects of the Self-Actuation and Motility of Thermosalient Crystals. *J. Am. Chem. Soc.* **2013**, *135*, 12241–12251.

[14] Bernstein, J. *Polymorphism in molecular crystals*; International Union of Crystallography Book Series (Volume 14); Oxford University Press: New York, 2002.

[15] Timmermans, J. Plastic Crystals: A Historical Review. *J. Phys. Chem. Solids* **1961**, *18*, 1−8.

[16] Murrill, E.; Breed, L. Solid–Solid Phase Transitions Determined by Differential Scanning Calorimetry: Part I. Tetrahedral Substances. *Thermochim. Acta* **1970**, *1*, 239−246.

[17] *Crystallization Processes in Fats and Lipid Systems*; Garti, N., Sato, K., Eds.; CRC Press: Boca Raton, FL, 2001.

[18] Görbitz, C. H. Solid-State Phase Transitions in dl-Norvaline Studied by Single-Crystal X-ray Diffraction. *J. Phys. Chem. B* **2011**, *115*, 2447−2453.

[19] Smets, M. M. H.; Brugman, S. J. T.; van Eck, E. R. H.; van den Ende, J. A.; Meeks, H.; Cuppen, H. M. Understanding the Solid-State Phase Transitions of dl-Norleucine: An in Situ DSC, Microscopy, and Solid-State NMR Study. *Cryst. Growth Des*. **2015**, *15*, 5157−5167.

[20] Anwar, J.; Tuble, S. C.; Kendrick, J. Concerted Molecular Displacements in a Thermally-Induced Solid-State Transformation in Crystals of dl-Norleucine. *J. Am. Chem. Soc.* **2007**, *129*, 2542−2547.

[21] Chung, H.; Ruzié, C.; Geerts, Y.; Diao, Y. Hybrid Mechanism of Nucleation and Cooperative Propagation in a Single-Crystal-to-Single-Crystal Transition of a Molecular Crystal. *Cryst. Growth Des.* **2018**, *18*, 4245−4251.

[22] Chung, H.; Dudenko, D.; Zhang, F.; D'Avino, G.; Ruzié, C.; Richard, A.; Schweicher, G.; Cornil, J.; Beljonne, D.; Geerts, Y.; Diao, Y. Rotator Side Chains Trigger Cooperative Transition for Shape and Function Memory Effect in Organic Semiconductors. *Nat. Comm.* **2018**, *9*, 278.

[23] Barton, L. M.; Edwards, J. T.; Johnson, E. C.; Bukowski, E. J.; Sausa, R. C.; Byrd, E. F. C.; Orlicki, J. A.; Sabatini, J. J.; Baran, P. S. Impact of Sterero- and Regiochemistry on Energetic Materials. *J. Am. Chem. Soc.* **2019**, *141*, 12531−12535.

[24] Nepali, K.; Lee, H.-Y.; Liou, J.-P. Nitro-Group-Containing Drugs. *J. Med. Chem.* **2019**, *62*, 2851−2893.

[25] Formenti, D.; Ferretti, F.; Scharnagl, F. K.; Beller, M. Reduction of Nitro Compounds Using 3d-Non-Noble Metal Catalysts. *Chem. Rev.* **2019**, *119*, 2611-2680.

[26] Yu, C.; Fu, J.; Muzzio, M.; Shen, T.; Su, D.; Zhu, J.; Sun, S. CuNi Nanoparticles Assembled on Graphene for Catalytic Methanolysis of Ammonia Borane and Hydrogenation of Nitro/Nitrile Compounds. *Chem. Mater.* **2017**, *29*, 1413-1418.

[27] Whitaker, C. M.; Patterson, E. V.; Kott, K. L.; McMahon, R. J. Nitrogen and Oxygen Donors in Nonlinear Optical Materials: Effects of Alkyl vs Phenyl Substitution on the Molecular Hyperpolarizability. *J. Am. Chem. Soc.* **1996**, *118*, 9966−9973.

[28] Kenis, P. J. A.; Noordman, O. F. J.; Houbrechts, S.; van Hummel, G. J.; Harkema, S.; van Veggel, F. C. J. M.; Clays, K.; Engbersen, J. F. J.; Persoons, A.; van Hulst, N. F.; Reinhoudt, D. N. Second-Order Nonlinear Optical Properties of the Four Tetranitrotetrapropoxycalix[4]arene Conformers. *J. Am. Chem. Soc.* **1998**, *120*, 7875−7883.

[29] Baitinger, W. F.; Schleyer, P. von R.; Murty, T. S. S. R.; Robinson, L. Nitro Groups as Proton Acceptors in Hydrogen Bonding. *Tetrahedron* **1964**, *20*, 1635−1647.

[30] Abraham, M. H.; Platts, J. A. Hydrogen Bond Structural Group Constants. *J. Org. Chem.* **2001**, *66*, 3484−3491.

[31] Etter, M. C. Encoding and Decoding Hydrogen-Bond Patterns of Organic Compounds. *Acc. Chem. Res*. **1990**, *23*, 120−126.

[32] Allen, F. H.; Baalham, C. A.; Lommerse, J. P. M.; Raithby, P, R.; Sparr, E. Hydrogen-Bond Acceptor Properties of Nitro-O Atoms: A Combined Crystallographic Database and *Ab Initio* Molecular Orbital Study. *Acta Cryst.* **1997**, *B53*, 1017−1024.

[33] Robinson, J. M. A.; Philp, D.; Harris, K. D. M.; Kariuki, B. M. Weak Interactions in Crystal Engineering – Understanding the Recognition Properties of the Nitro Group. *New J. Chem*. **2000**, *24*, 799−806.

[34] Trueblood, K. N.; Goldish, E.; Donohue, J. A Three-Dimensional Refinement of the Crystal Structure of 4-Nitroaniline. *Acta Cryst.* **1961**, *14*, 1009−1017.

[35] Chen, P. C.; Chen, S. C. Theoretical Study of the Internal Rotational Barriers in Nitrobenzene, 2-Nitrotoluene, 2-Nitrophenol, and 2-Nitroaniline. *Int. J. Quantum Chem.* **2001**, *83*, 332−337.

[36] Sancho-Garćia, J. C.; Pérez-Jiménez, A. J. Nitrobenzene Rotational Energy Barrier: A Survey of Several *ab initio* Methods. *J. Chem. Phys.* **2003**, *119*, 5121−5127.

[37] Panunto, T. W.; Urbánczyk-Lipkowska, Z.; Johnson, R.; Etter, M. C. Hydrogen-Bond Formation in Nitroanilines: The First Step in Designing Acentric Materials. *J. Am. Chem. Soc.* **1987**, *109*, 7786−7797.

[38] Cohen, M. D.; Schmidt, G. M. J. Topochemistry. Part I. A Survey. *J. Chem. Soc.* **1964**, 1996−2000.

[39] Bernstein, J. Crystal Growth, Polymorphism and Structure−Property Relationships in Organic Crystals. *J. Phys. D: Appl. Phys.* **1993**, *26*, B66−B76.

[40] Saha, S.; Mishra, M. K.; Reddy, C. M.; Desiraju, G. R. From Molecules to Interactions to Crystal Engineering: Mechanical Properties of Organic Solids. *Acc. Chem. Res*. **2018**, *51*, 2957−2967.

[41] Yu, L. Polymorphism in Molecular Solids: An Extraordinary System of Red, Orange, and Yellow Crystals. *Acc. Chem. Res*. **2010**, *43*, 1257−1266.

[42] Edraki, N.; Mehdipour, A. R.; Khoshneviszadeh, M.; Miri, R. Dihydropyridines: Evaluation of Their Current and Future Pharmacological Applications. *Drug Discov. Today* **2009**, *14*, 1058−1066.

[43] Echert, T.; Müller, J. Über polymorphe Modifikationen des Nifedipine aus unterkühlten Schmelzen. *Arch. Pharm*. **1977**, *310*, 116−118.

[44] Triggle, A. M.; Shefter, E.; Triggle, D. J. Crystal Structures of Calcium Channel Antagonists: 2,6-Dimethyl-3,5-Dicarbomethoxy-4-[2-Nitro-, 3-Cyano-, 4-(Dimethylamino)-, and 2,3,4,5,6-Pentafluorophenyl]-1,4-Dihydropyridine. *J. Med. Chem.* **1980**, *23*, 1442−1445.

[45] Burger, A.; Koller, K. T. Polymorphism and Pseudopolymorphism on Nifedipine. *Sci. Pharm*. **1996**, *64*, 293−301.

[46] Bortolotti, M.; Lonardelli, I.; Pepponi, G. Determination of the Crystal Structure of Nifedipine Form C by Synchrotron Powder Diffraction. *Acta Cryst.* **2011**, *B67*, 357−364.

[47] Gunn, E.; Guzei, I. A.; Cai, T.; Yu, L. Polymorphism of Nifedipine: Crystal Structure and Reversible Transition of the Metastable β Polymorph. *Cryst. Growth Des*. **2012**, *12*, 2037−2043.

[48] Cruz-Cabeza, A. J.; Bernstein, J. Conformational Polymorphism. *Chem. Rev.* **2014**, *114*, 2170−2191.

[49] Mitchell, C. A.; Yu, L.; Ward, M. D. Selective Nucleation and Discovery of Organic Polymorphs through Epitaxy with Single Crystal Substrates. *J. Am. Chem. Soc.* **2001**, *123*, 10830−10839.

[50] Lévesque, A.; Maris, T.; Wuest, J. D. ROY Reclaims Its Crown: New Ways to Increase Polymorphic Diversity. *J. Am. Chem. Soc.* **2020**, *142*, 11873−11883.

[51] Surov, A. O.; Solanko, K. A.; Bond, A. D.; Perlovich, G. L.; Bauer-Brandl, A. Crystallization and Polymorphism of Felodipine. *Cryst. Growth Des.* **2012**, *12*, 4022−4030.

[52] Triggle, D. J.; Langs, D. A.; Janis, R. A. Ca^{2+} Channel Ligands: Structure-Function Relationships of the 1,4-Dihydropyridines. *Med. Res. Rev.* **1989**, *9*, 123−180.

[53] Kappe, C. O.; Fabian, W. M. F. Conformational Analysis of 4-Aryl-Dihydropyrimidine Calcium Channel Modulators. A Comparison of Ab Initio, Semiempirical and X-Ray Crystallographic Studies. *Tetrahedron* **1997**, *53*, 2803−2816.

[54] Su, Y.; Xu, J.; Shi, Q.; Yu, L.; Cai, T. Polymorphism of Griseofulvin: Concomitant Crystallization from the Melt and a Single Crystal Structure of a Metastable Polymorph with Anomalously Large Thermal Expansion. *Chem. Comm.* **2018**, *54*, 358−361.

[55] Apperley, D. C.; Forster, A. H.; Fournier, R.; Harris, R. K.; Hodgkinson, P.; Lancaster, R. W.; Rades, T. Characterisation of Indomethacin and Nifedipine Using Variable-Temperature Solid-State NMR. *Magn. Reson. Chem*. **2005**, *43*, 881−892.

[56] Lu, M. CCDC 1893050: Experimental Crystal Structure Determination, 2019, DOI: 10.5517/ccdc.csd.cc21jw4m

[57] Yu, L. Inferring Thermodynamic Stability Relationship of Polymorphs from Melting Data. *J. Pharm. Sci*. **1995**, *84*, 966−974.

[58] Grooff, D.; De Villiers, M. M.; Liebenberg, W. Thermal Methods for Evaluating Polymorphic Transitions in Nifedipine. *Thermochim. Acta* **2007**, *454*, 33−42.

[59] Marsac, P, J.; Konno, H.; Taylor, L. S. A Comparison of the Physical Stability of Amorphous Felodipine and Nifedipine Systems. *Pharm. Res.* **2006**, *23*, 2306−2316.

[60] Panda, M. K.; Runčevski, T.; Husain, A.; Dinnebier, R. E.; Naumov, P. Perpetually Self-Propelling Chiral Single Crystals. *J. Am. Chem. Soc*. **2015**, *137*, 1895−1902.

[61] Fossheim, R.; Solo, J. A. J.; Luchowski, E.; Rutledge, A.; Triggle, D. J. Crystal Structures and Pharmacologic Activities of 1,4-Dihydropyridine Calcium Channel Antagonists of the Isobutyl Methyl 2,6-Dimethyl-4-(Substituted Phenyl)-1.4-Dihydropyridine-3,5-Dicarboxylate (Nisoldipine) Series. *J. Med. Chem.* **1988**, *31*, 300-305.

[62] Andrews, D. H. The Specific Heats of Some Isomers of the Type Ortho, Meta and Para C_6H_4XY from 110° to 340 °K. *J. Am. Chem. Soc.* **1926**, *48*, 1287−1298.

[63] CSD Ref. Code NANILI for *para*-nitroaniline, MNIANL for *meta*-nitroaniline, ONITAN for *ortho*-nitroaniline.

[64] Fábry, J.; Dušek, M.; Vaněk, P.; Rafalovskyi, I.; Hlinka, J.; Urban, J. High- and Low-Temperature Phases in Isostructural 4-Chloro-3-Nitroaniline and 4-Iodo-3-Nitroaniline. *Acta Cryst.* **2014**, *C70*, 1153−1160.

[65] Graham, D.; Kennedy, A. R.; McHugh, C. J.; Smith, W. E.; David, W. I. F.; Shankland, K.; Shankland, N. The Crystal Structures of Three Primary Products from the Selective Reduction of 2,4,6-Trinitrotoluene. *New. J. Chem.* **2004**, *28*, 161−165.

[66] Mnyukh, Y. V.; Panfilova, N. A.; Petropavlov, N. N.; Uchvatova, N. S. Polymorphic Transitions in Molecular Crystals – III. Transitions Exhibiting Unusual Behavior. *J. Phys. Chem. Solids* **1975**, *36*, 127−144.

[67] Beckham, G. T.; Peters, B; Starbuck, C.; Variankaval, N.; Trout, B. L. Surface-Mediated Nucleation in the Solid-State Polymorph Transformation of Terephthalic Acid. *J. Am. Chem. Soc.* **2007**, *129*, 4714−4723.

[68] Schmidt, J. R.; Polik, W. F. *WebMO Enterprise*, version 19.0; WebMO LLC: Holland, MI, USA, 2019; http://www.webmo.net (accessed March, 2019).

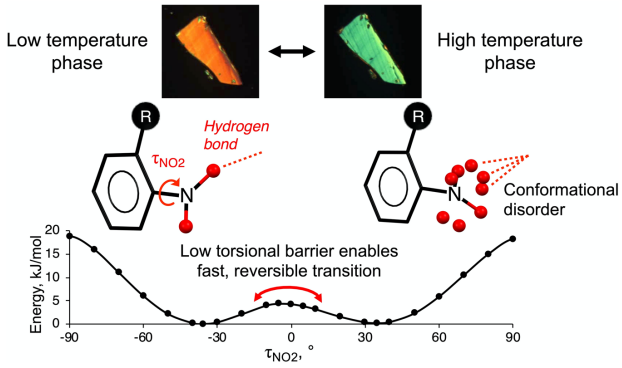
Low temperature phase
High temperature phase
R
Hydrogen bond
τNO2
N
R
N
Conformational disorder
Low torsional barrier enables fast, reversible transition
Energy, kJ/mol
20
15
10
5
0
-90
-60
-30
0
30
60
90
τNO2, °